Human Influence on Seasonal Precipitation in Europe

NIKOLAOS CHRISTIDIS[a] AND PETER A STOTT[a]

[a] *Met Office Hadley Centre, Exeter, United Kingdom*

(Manuscript received 23 August 2021, in final form 29 March 2022)

ABSTRACT: The response of precipitation to global warming is manifest in the strengthening of the hydrological cycle but can be complex on regional scales. Fingerprinting analyses have so far detected the effect of human influence on regional changes of precipitation extremes. Here we examine changes in seasonal precipitation in Europe since the beginning of the twentieth century and use an ensemble of new climate models to assess the role of different climatic forcings, both natural and anthropogenic. We find that human influence gives rise to a characteristic pattern of contrasting trends, with drier seasons in the Mediterranean basin and wetter over the rest of the continent. The trends are stronger in winter and weaker in summer, when drying is more spatially widespread. The anthropogenic signal is dominated by the response to greenhouse gas emissions, but is also weakened, to some extent, by the opposite effect of anthropogenic aerosols. Using a formal fingerprinting attribution methodology, we show here for the first time that the effects of the total anthropogenic forcing, and also of its greenhouse gas component, can be detected in observed changes of winter precipitation. Greenhouse gas emissions are also found to drive an increase in precipitation variability in all seasons. Moreover, the models suggest that human influence alters characteristics of seasonal extremes, with the frequency of high precipitation extremes increasing everywhere except the Mediterranean basin, where low precipitation extremes become more common. Regional attribution information contributes to the scientific basis that can help European citizens build their climate resilience.

KEYWORDS: Europe; Precipitation; Anthropogenic effects/forcing; Climate change; Pattern detection; Climate models

1. Introduction

Scientific evidence makes it clear that a warming climate engenders changes in precipitation around the world (Bindoff et al. 2013). On a global scale, as surface temperature rises, water vapor increases at a rate of 6%–7% per Celsius degree (Trenberth 2011). This leads to an intensification of the hydrological cycle, though regional hydroclimatic changes may be more complex than a mere amplification of existing patterns (Allan 2014; Kumar et al. 2015). The change in global precipitation itself is not only driven by moisture but also by the energy budget of the troposphere and has been suggested to evolve at a lower rate (Allen and Ingram 2002; Held and Soden 2006).Understanding modifications in precipitation patterns is crucial, as they are associated with a raft of socioeconomic impacts, like, for example, loss of lives and livelihood due to an increasing risk of droughts or floods (Wilhite et al. 2007; Dottori et al. 2018). Taking a closer look at Europe, summer droughts of unprecedented severity in the Mediterranean region are projected to become common by the end of the century (Christidis and Stott 2021), which highlights that even in countries with a relatively high adaptive capacity, communities may still be greatly vulnerable.

How well do climate models represent changes in precipitation? On a global scale, Polson and Hegerl (2017) demonstrate that models that contributed to phase 5 of the Coupled Model Intercomparison Project (CMIP5; Taylor et al. 2012) simulate an intensification of the water cycle consistent with observed data. CMIP5 models have also been shown to represent well post-1948 zonal trend precipitation patterns over land, including a rainfall increase in Northern Hemisphere midlatitudes, though the trends are weaker than the observations suggest (Li et al. 2016). The new generation of CMIP6 models (Eyring et al. 2016) brings in further improvements (Bock et al. 2020; Vannière et al. 2019), including a better representation of storm tracks in the North Atlantic (Priestley et al. 2020), pertinent to European rainfall.

Trends in regional precipitation can be driven by a combination of forced thermodynamical and dynamical changes (Seager et al. 2010) and may be more challenging for models to simulate because of higher natural variability, as well as the rudimentary representation of small-scale processes (Jakob 2014). An example of the complexity in the interaction between different drivers is the increase in winter European rainfall, influenced by changes in the storm tracks, which in turn are affected by changes in stratospheric circulation (Scaife et al. 2012). In contrast, the Mediterranean region becomes drier in winter and tropical influences have been identified as

Denotes content that is immediately available upon publication as open access.

Supplemental information related to this paper is available at the Journals Online website: https://doi.org/10.1175/JCLI-D-21-0637.s1.

Corresponding author: Nikolaos Christidis, nikos.christidis@metoffice.gov.uk

DOI: 10.1175/JCLI-D-21-0637.1

a possible mechanism for this change (Hoerling et al. 2012). Finally, observational uncertainties could pose an additional setback in model evaluation (Bhend and Whetton 2013). Despite modeling challenges Knutson and Zeng (2018) demonstrated that CMIP5 models yield realistic regional precipitation trends and reported consistency with the observations in most areas. It has also been claimed that spatial characteristics of the response to climatic forcings may in fact render certain regional changes more detectable (Sarojini et al. 2016).

Attribution studies set out to establish whether the effect of external, and, in particular, anthropogenic forcings can be detected in observed climatic changes. While the Fifth Assessment Report (AR5) of the Intergovernmental Panel on Climate Change (IPCC) concluded there is high confidence that human influence has contributed to the recent warming on global to continental scales, medium confidence was assigned with regard to precipitation changes over land, including increases in the Northern Hemisphere's mid- and high latitudes (Bindoff et al. 2013). However, more recent studies strengthened this attribution statement, which is assigned high confidence in the latest Sixth Assessment Report (AR6; Eyring et al. 2021). There is stronger evidence for detection of the anthropogenic effect on large-scale changes, including the strengthening of the hydrological cycle (Wu et al. 2013; Padrón et al. 2020) or zonal trends (Zhang et al. 2007). Detection has also been shown for annual and seasonal precipitation trends in northern high latitudes where snow/ice feedback give rise to a stronger signal (Wan et al. 2015). Regional effects, however, have been more difficult to detect (Sarojini et al. 2016). The need for regional attribution studies is pressing, as they provide information that is most useful in helping communities reduce their vulnerability to climate change. Christidis and Stott (2021) provided some first insights into summer rainfall changes in Europe due to human activity and identified an opposite response in the drying Mediterranean region and the rest of the continent where rainfall increases. Here we take a step farther and examine whether this characteristic nonuniform pattern is present in other seasons too and whether the fingerprint of human activity can be detected. Formal detection on regional scales has not been shown yet for changes in seasonal mean precipitation.

Changes in extreme precipitation do not necessarily arise the same way as the mean and human influence may be arguably easier to detect in this case. Thermodynamical drivers linked to moisture and ultimately temperature changes play a major role in the intensification of extremes, which can more confidently be attributed to anthropogenic forcings (Pendergrass et al. 2015). Rainfall extremes have been shown to increase in most parts of the world (Alexander 2016) and recent trends have been attributed to human influence both globally and on continental regions, including Europe, China, and North America (Madakumbura et al. 2021; Dong et al. 2021; Chen and Sun 2017; Kirchmeier-Young and Zhang 2020). As greenhouse gas emissions continue to rise, their weaker effect on mean precipitation is also expected to emerge above variability. Our study aims to assess whether detection of a seasonal signal is already possible in the wider area of Europe on the basis of a formal attribution fingerprinting method.

We here employ a suite of CMIP6 models and rainfall observations to examine the contributions of different external forcings, both natural and anthropogenic, to seasonal precipitation trends in Europe since the beginning of the twentieth century. We partition the overall anthropogenic effect between different forcing components like greenhouse gas and aerosol emissions and investigate the detectability of the climate's response in the observations with a fingerprinting attribution technique. The impact of human influence on extremes of seasonal rainfall is also investigated, calling attention to the contrast between the northern and southern parts of the continent. Although, as an attribution study, the focus is kept on past changes, future changes in European precipitation are also briefly considered.

The remainder of the paper is organized as follows: in section 2 we list the data used in the analysis and explain how they were processed. Section 3 presents the observed and simulated changes in European precipitation, considering both long term trends as well as changes in variability. The detectability of the influence of anthropogenic forcings on observed seasonal rainfall changes is assessed in section 4. Section 5 discusses the changing characteristics of seasonal extremes. The main results and concluding remarks are given in section 6.

2. Data

We employ fields of gridded monthly precipitation over land from Climatic Research Unit (CRU) time series (TS), version 4.03 (CRU TS4.03), a dataset constructed with observations during the period 1901–2018 (Harris et al. 2020). The fields, which cover all land areas except Antarctica, are homogenized and available on a 0.5° latitude by 0.5° longitude grid. Uncertainties associated with orographic correction and interpolation techniques may pose limitations in assessments of local changes but are expected to have little effect on our results, which concentrate on larger spatial scales. Unlike station data, the gridded dataset also allows us to examine patterns of change across the whole continent in a uniform manner. Harris et al. (2020) also demonstrate that the coverage of European observations is good even in earlier years. Although the limited length of the observational record and the effect of natural variability pose limitations to the evaluation of climate models, CRT TS4 data can still provide a useful test bed for a simple assessment of simulated precipitation characteristics. Moreover, application of an optimal detection methodology in section 4 will help establish in a more rigorous statistical framework whether simulated signals of forced climate change are detectable in the observations.

Simulated monthly precipitation data come from experiments with a multimodel ensemble of 9 CMIP6 models (Table 1). Each model provides multiple simulations for each experiment. We selected only those models that provide data for all the experiments utilized in this study. For a basic attribution assessment, we compare simulations with and without human influence on the climate. The former come from an experiment with all forcings (ALL), that is, both anthropogenic and natural, while the latter come from an experiment that includes only changes in volcanic aerosols and the solar irradiance (NAT).

TABLE 1. The CMIP6 models and the experiments used in the study. The number of simulations employed in the analysis for each model and each experiment is shown in the table. The ALL experiment was extended to year 2100 with SSP2 4.5. The total number of simulations per experiment is given in the last row.

	Model	ALL+ SSP2 4.5	NAT	GHG	AER
1	BCC-CSM2-MR	1	3	3	3
2	CNRM-CM6.1	6	10	10	10
3	CanESM5	25	15	25	15
4	GFDL-ESM4	3	3	1	1
5	HadGEM3-GC3.1-LL	1	4	4	4
6	IPSL-CM6A-LR	9	10	10	10
7	MIROC6	3	3	3	3
8	MRI-ESM2.0	1	5	5	5
9	NorESM2-LM	3	3	3	3
	Total	52	56	64	54

The total anthropogenic effect (ANTHRO) in CMIP6 simulations represents the effect of changes in well-mixed greenhouse gases, aerosols, ozone, and land use. We break down the ANTHRO component further and also examine the response to greenhouse gas and aerosol emissions separately, using CMIP6 experiments that only simulate the effect of these forcings (GHG and AER, respectively). This distinction between GHG and AER is of particular interest as the two forcings may lead to opposite rainfall trends (Wu et al. 2013). Future changes are considered by extending the ALL simulations from year 2015 to the end of the twenty-first century with the "middle of the road" Shared Socioeconomic Pathway 2 4.5 (SSP2 4.5; Riahi et al. 2017). The remaining experiments provide simulations up to year 2020, and all of the simulations start in year 1850. Our attribution analysis also requires simulations of a "control" climate (CTL) without the effect of any external forcings, which approximates the preindustrial climate. The models also provide such long CTL simulations, from which we extract about 6200 years of data in total.

The CMIP6 data were processed in standard ways to be fit for use in a multimodel analysis. The simulated fields are regridded onto the CRU TS4 grid and also masked with the observations to include land areas only. For a meaningful comparison between different models that may have different mean biases, we report seasonal precipitation as an anomaly relative to the baseline period 1901–1930. The choice of an early period, serving as a proxy of the preindustrial climate, is deliberate and common in attribution studies (Bindoff et al. 2013), as it allows us to account for the bulk of the anthropogenic effect. A key advantage of large multimodel ensembles is that the ensemble mean offers a clearer representation of forced changes, as averaging suppresses the effect of internal climate variability. On the other hand, no multimodel ensemble is perfectly constructed, and any analysis is limited by the suite of available models, often referred to as "an ensemble of opportunity." In our study it is evident that the models we

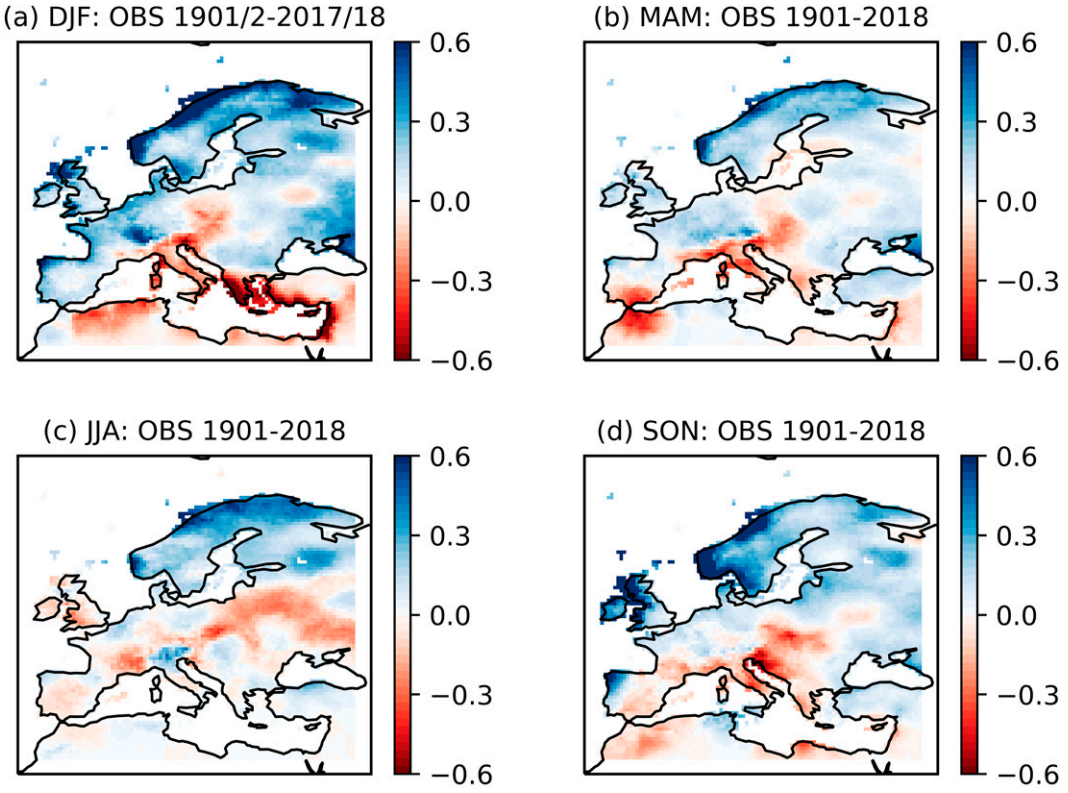

FIG. 1. Seasonal precipitation trends (mm yr^{-1}) calculated with CRU TS4 data over 1901–2018. Each panel corresponds to a different season, marked in the title by the first letters of the months within the season.

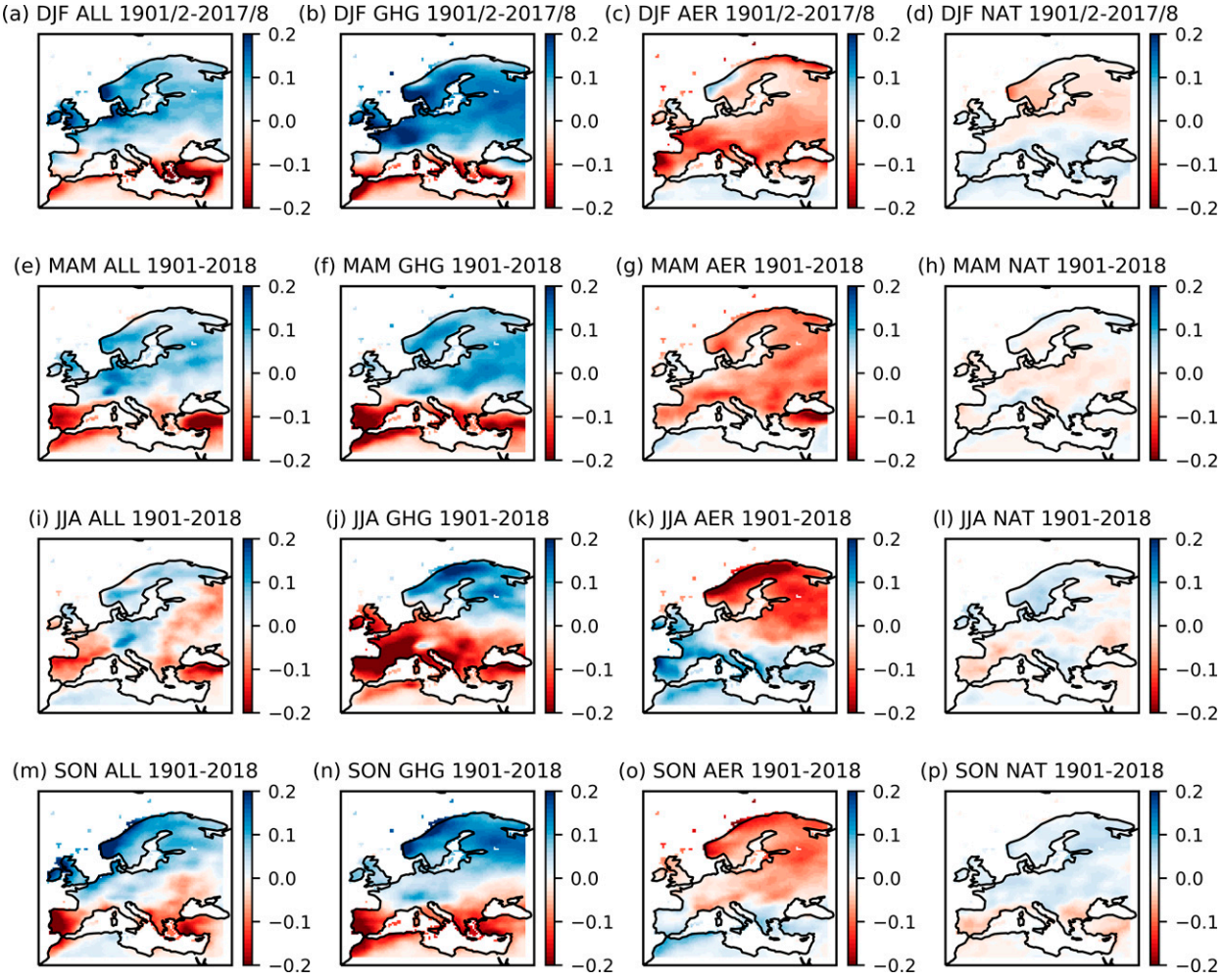

FIG. 2. Seasonal precipitation trends (mm yr^{-1}) calculated with data from different CMIP6 experiments over the observational period. The patterns correspond to the weighted ensemble mean for experiments (a),(e),(i),(m) ALL, (b),(f),(j),(n) GHG, (c),(g),(k),(o) AER, and (d),(h),(l),(p) NAT. Different rows of panels correspond to different seasons, as marked in the titles.

employ make an unequal contribution to the ensemble mean, and consequently a simple averaging would give greater weight to models with the largest number of simulations (CanESM5, CNRM, and IPSL). Hence, as in previous multimodel attribution studies (e.g., Jones et al. 2013), we construct the multimodel ensemble mean for each experiment by assigning equal weight to all models. The weight is calculated as the inverse of the number of simulations provided by the model for the reference experiment multiplied by the inverse of the number of different models. The resultant weighted ensemble mean is the equivalent of taking the average of all the models' ensemble averages.

Changes in precipitation are investigated over the wider European area 10°W—40°E, 30°—75°N, which is made up of the two predefined, subcontinental "Giorgi" regions (Giorgi and Francisco 2000) of northern Europe (NEU) and the Mediterranean basin (MED). The Giorgi regions were introduced to represent different climatic regimes and physiographic settings over spatial scales that are well captured by the majority of climate models. Here we examine spatial patterns of change over the reference European area as well as mean changes in the NEU and MED regions. Spatial divisions over smaller regions act as a form of spatial smoothing that aims to improve signal detectability. There are of course different ways such divisions can be made. It is important to bear in mind that the selected regions should be small enough to provide sufficient information that helps our attribution tools distinguish between different forcings, but also large enough to minimize the effect of internal variability. We find here that division into two subcontinental regions maximizes the signal-to-noise ratio, and hence the Giorgi regions are more suitable than, for example, the AR6 reference regions (Iturbide et al. 2020) that split Europe into three areas. Complexities of the European climate would require consideration of smaller local scales, in the context, for example, of analyses with regional, or convection-permitting models, which we propose as complementary follow-up work. Here we start by considering larger scales and we will next present seasonal changes

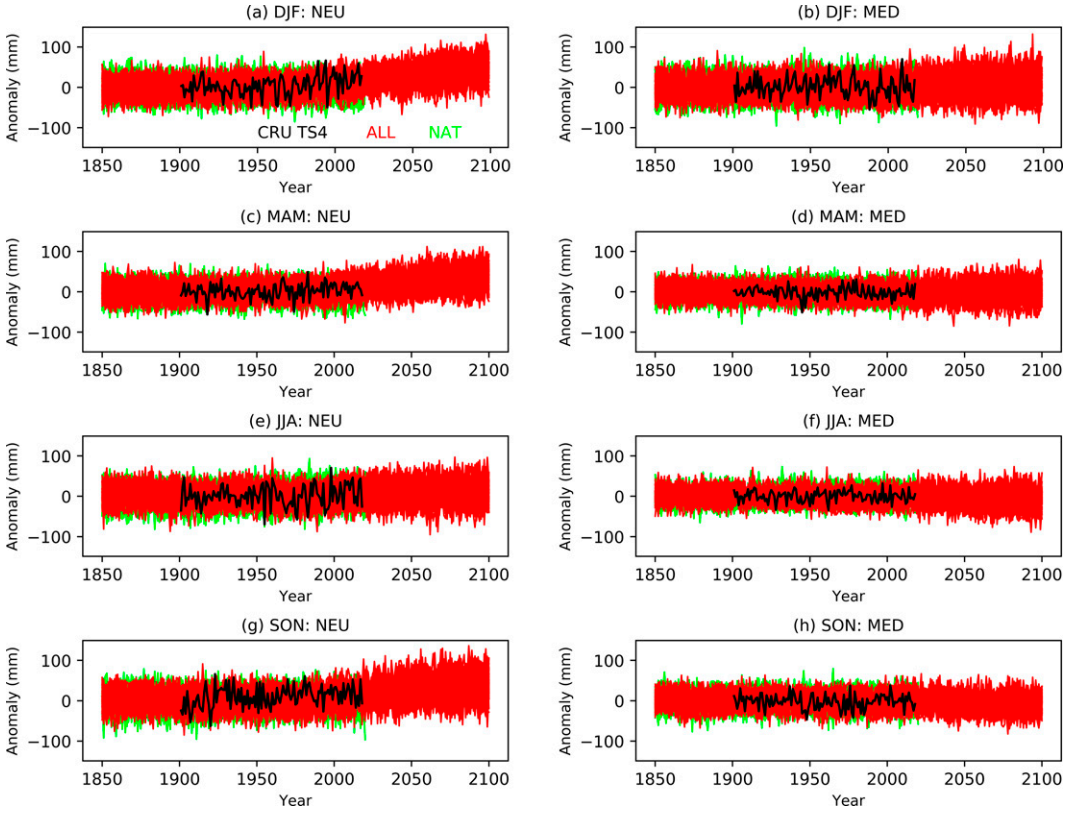

FIG. 3. Time series of seasonal mean precipitation anomalies relative to 1901–30 computed with observational data (black) and data from the CMIP6 simulations with (red) and without (green) the effect of human influence. Anomalies are averaged over (a),(c),(e),(g) the NEU region and (b),(d),(f),(h) the MED region. Different rows of panels correspond to different seasons, as marked in the titles.

inferred from the CMIP6 models and the observations and will also provide a simple first assessment of the contributions of different forcings.

3. Observed and simulated precipitation changes

a. Trend patterns

We first construct seasonal precipitation trend patterns over the observational period 1901–2018 with CRU TS4 data (Fig. 1). We find a mix of positive and negative trends in different parts of the continent, but also note a possible signal of rainfall decreases in the Mediterranean area and increases over most other parts of the continent, with the exception of summer, where drying is more widespread and rainfall increases are mainly concentrated in Scandinavia. It should be stressed, however, that observed trends are expected to be highly influenced by natural variability, which partly obscures the effect of forced changes. To assess the latter, we also construct trend patterns from the (weighted) multimodel ensemble mean for all the CMIP6 experiments considered in this study (Fig. 2). As averaging suppresses to some extent the effect of internal variability, the resulting patterns are more uniform, and the mean trends are also smaller than the observed trends. The ALL trends (Figs. 2a,e,i,m) illustrate more clearly the north–south contrast, as well as the more widespread drying in summer, and to a smaller degree in autumn, which extends over parts of eastern Europe. The NAT experiment yields smaller trends, suggesting that the total forced response is primarily driven by anthropogenic forcings. Knutson and Zeng (2018) also find a north–south contrast in annual precipitation trends in Europe and, using CMIP5 runs of the preindustrial climate, demonstrate the significance of this pattern.

Although it is beyond the scope of our study to identify physical processes or thermodynamical and dynamical mechanisms that operate behind the forced response to external forcings, previous research offers some valuable insights. The drying of the Mediterranean region has been suggested to be mainly of thermodynamical origin and linked to the land–sea warming contrast, changes in the lapse rate, and land–atmosphere interactions (Brogli et al. 2019; Barcikowska et al. 2020). Dynamical drivers have also been proposed for winter changes in the region including changes in circulation and teleconnections (Brogli et al. 2019; Hoerling et al. 2012). Increasing precipitation in the northern parts of the continent, on the other hand, may predominantly be of dynamical origin and influenced, for example, by a southward shift of the jet stream due to sea ice losses (Screen 2013). While further research is

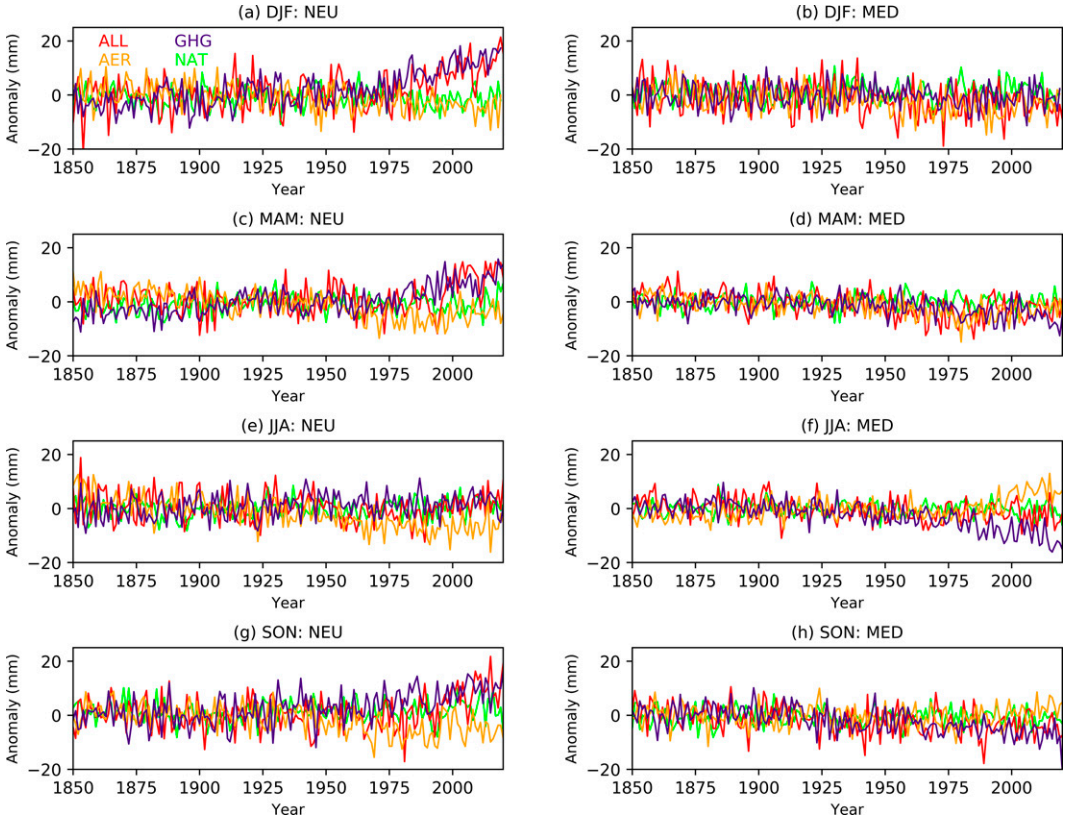

FIG. 4. Time series of seasonal mean precipitation anomalies relative to 1901–30 corresponding to the weighted ensemble mean of the ALL (red), GHG (purple), AER (orange), and NAT (green) experiments. Anomalies are averaged over (a),(c),(e),(g) the NEU region and (b),(d),(f),(h) the MED region. Different rows of panels correspond to different seasons, as marked in the titles.

needed to examine the models' ability to represent the above processes, the overall consistency between modeled and observed changes is reassuring.

Precipitation changes in response to greenhouse gas and aerosol emissions separately are also depicted in Fig. 2. The ALL and GHG patters have similar shapes with the exception of summer when rainfall decreases extend northward in the GHG experiment. The GHG trends, however, are greater than ALL. This suggests that while greenhouse gas emissions appear to dominate the overall change, their effect is somewhat tempered. This trend reduction may be explained by the effect of aerosol emissions, which, according to the models, leads to a continent-wide decrease in rainfall in winter and spring and to a response opposite of GHG in summer and autumn. This contrast between precipitation changes in GHG and AER experiments was also seen in larger-scale changes over the Northern Hemisphere and the fingerprint of the two opposing forcings was detected in post-1950 observations (Wu et al. 2013). While greenhouse gas emissions increase the longwave radiation at the surface, aerosol emissions reduce the shortwave radiation through scattering (direct effect) and the modification of cloud properties (indirect effect). The interplay between the two forcings determines the total response, and as European aerosols emissions decrease, the greenhouse gas influence is expected to intensify in coming years (Westervelt et al. 2018).

b. *Changes in NEU and MED and variability evaluation*

We next examine temporal changes in seasonal precipitation averaged over the NEU (10°W–40°E, 50°–75°N) and MED (10°W–40°E, 30°–50°N) regions. Time series of seasonal anomalies computed with CRU TS4, and the ALL and NAT simulations are shown in Fig. 3. Over the observational period, both CRU TS4 and the mean of the ALL simulations yield positive trends in NEU, indicating increases in precipitation, and small negative trends in MED, indicating drying. The NAT experiment gives near-zero trends, and the NAT time series are hardly distinguished from the ALL, as they both mainly reflect the effect of natural variations, though in more recent years changes in the ALL experiment become more prominent. In future decades, however, the NEU rainfall displays a clear increase in all seasons, with the larger change seen in winter. Despite the strong drying trends seen in parts of the Mediterranean area (Fig. 2), the MED time series do not show a clear decrease in precipitation, as the MED region is too large and therefore includes areas of both positive and negative trends that largely cancel out. The regional changes display the effects of both internal variability and

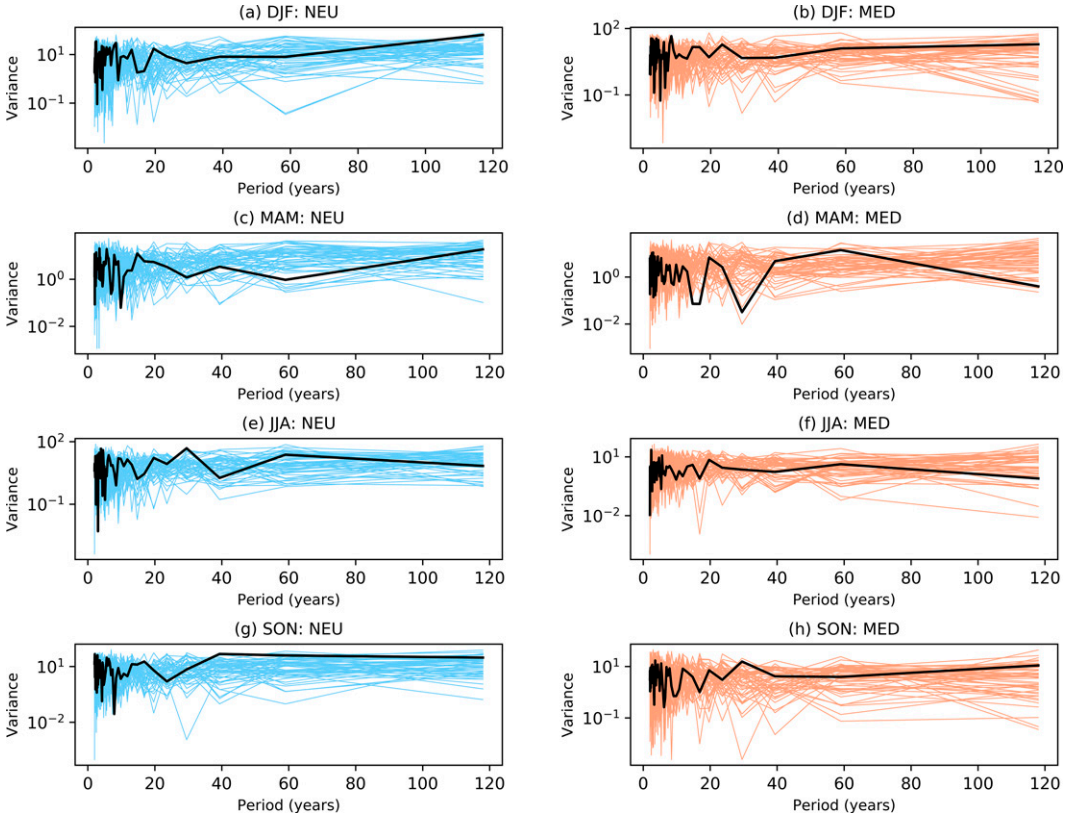

FIG. 5. Power spectra computed from seasonal precipitation time series (1901–2018) with data from observations (black) and simulations with all forcings (colored lines). Spectra are shown for (a),(c),(e),(g) the NEU region and (b),(d),(f),(h) the MED region. Different rows of panels correspond to different seasons, as marked in the titles.

external forcings and it has been suggested that model estimates of the latter may bear a low trend bias (Knutson and Zeng 2018) in models. The consistency between modeled forced signals and observed changes will be assessed later by our statistical attribution analysis. Trends over the observational period estimated with the CRU TS4 and different model experiments (ensemble mean) are reported in Table S1 in the online supplemental material. We stress, however, that the effect of internal variability, especially on observed trends, does not allow an instructive comparison.

To distinguish between different forcings, we also plot seasonal precipitation time series corresponding to the ensemble mean of each experiment (Fig. 4).We find that the overall (ALL) increase in NEU is very much a manifestation of the GHG response. Aerosol emissions induce an opposite response, which, however, is much weaker and thus not obvious in the ALL forced change. Interestingly, the GHG and AER responses are opposite in the MED region relative to NEU and are stronger in summer and autumn. The models suggest that greenhouse gas emissions drive a summer drying in the MED, which could be a direct response to warming, whereas aerosol emissions tend to increase rainfall, which might be indicative of the aerosol influence on cloud formation in a season that favors convective rainfall. Again, more work is needed to better understand the difference in the response to the two forcings. The overall effect is a weak summer drying in the MED, which could increase in strength, if the aerosol forcing were to become weaker.

Besides long-term trends, it is also important that models provide a realistic representation of natural variability across a range of time scales. Power spectra are often employed as a simple evaluation test in attribution studies (Gillett et al. 2000; Christidis et al. 2013). Spectra from seasonal precipitation time series based on observations and the 52 ALL simulations are shown in Fig. 5. The observed variability is found to lie within the range of the modeled variability and although the small observational sample does not allow a more conclusive assessment, the results indicate that the models employed in the study offer a reasonable representation and are thus fit for purpose. Spectra produced with detrended precipitation time series (to minimize the effect of external forcings) give qualitatively similar results. In comparing the observed and modeled standard deviation of seasonal precipitation during 1901–50, a period before the emergence of a prominent forced signal, we also find that the modeled range is consistent with the observations, as illustrated for DJF precipitation in Fig. S1 in the online supplemental material.

While power spectra offer an overall assessment of the simulated variability, a more focused look at some main modes of variability would also be useful. Trends and variability

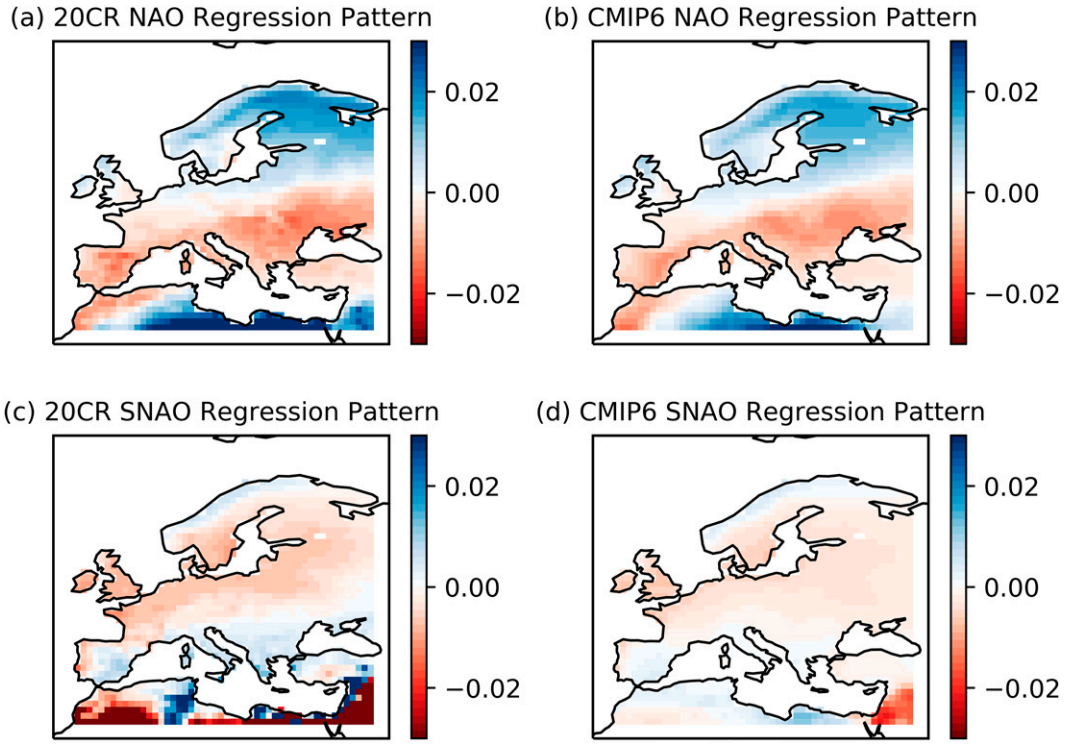

FIG. 6. Regression patterns showing (a),(b) the winter precipitation dependence on the NAO and (c),(d) the summer precipitation dependence on the SNAO. The patterns were constructed with (left) 20CR reanalysis data and (right) the ALL simulations. The ALL maps in (c) and(d) correspond to the weighted mean of the 52 patterns constructed with data from individual simulations.

associated with precipitation are the complex outcome of different processes, which cannot all be comprehensively assessed here. Therefore, in terms of atmospheric circulation influences, we concentrate on two main modes of winter and summer variability that affect the European climate, namely, the North Atlantic Oscillation (NAO; Hurrell et al. 2003) and the summer NAO (SNAO; Folland et al. 2009), and we assess how the CMIP6 models represent the precipitation response to these two seasonal oscillations.

We construct the NAO and SNAO indices using sea level pressure (SLP) data from the NOAA–CIRES–DOE Twentieth Century Reanalysis, version 3 (20CR; Slivinski et al. 2019), and the CMIP6 simulations of the ALL experiment. The indices are defined as the principal component (PC) of the leading EOF of winter and summer SLP anomalies over the North Atlantic (20°–80°N, 90°W–40°E) and are estimated here for the period 1850–2014 for which the 20CR data are available. The patterns of the leading EOF are computed with reanalysis data (Fig. S2 in the online supplemental material) and with pooled ALL data for each model. The principal component is then estimated for each year of the reference period with 20CR and the 52 ALL simulations. Regression maps that illustrate how the NAO and SNAO affect European precipitation in winter and summer, respectively, are subsequently constructed by regressing the gridpoint winter/summer precipitation against the NAO/SNAO index. We thus obtain patterns from 20CR and from each of the ALL model simulations. The reanalysis and the weighted ensemble mean regression patterns are shown in Fig. 6. Although the model patterns are smoother due to the ensemble averaging, they show a very similar precipitation response to the reanalysis, providing additional evidence of the adequacy of the CMIP6 models for our attribution analysis.

c. *Changes in variability*

While forced trends would lead to a shift of the precipitation distribution, changes in variability would also alter its shape, and the combination of the two is key for understanding how extremes, that is, events in the tails of the distribution, might be affected in a changing climate. Christidis and Stott (2021) showed that as European summers become warmer, there is an increase in summer rainfall variability, leading to a broadening of its distribution, which increases the likelihood of wet extremes, even in areas where summer rainfall decreases on the whole. Here we extend previous work and further investigate whether changes in variability are also manifest in other seasons, and also use the different CMIP6 experiments to determine how different forcings may contribute to the change.

Patterns of variability change in Europe constructed with observational data and the ALL simulations are illustrated in Fig. 7. The patterns depict the difference in the mean standard deviation of seasonal precipitation between the first and last

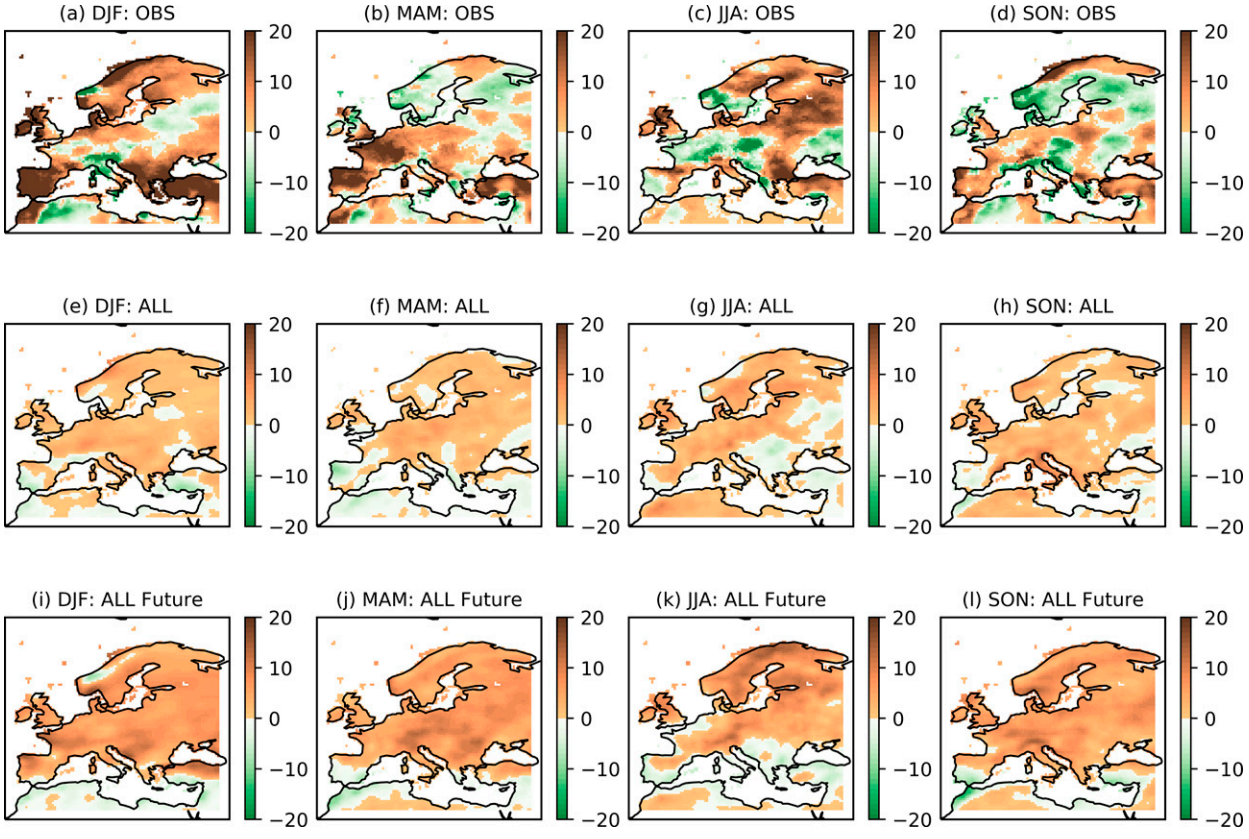

FIG. 7. Changes in the variability of seasonal precipitation. The mean standard deviation of seasonal precipitation is computed in the first and last 30 years of the observational period, and (a)–(d) their difference (recent minus earlier period) is shown. (e)–(h) Patterns computed in a similar way as in (a)–(d), but for the ALL experiment. The ALL maps correspond to the weighted mean of the 52 patterns constructed with individual simulations. (i)–(l) Future changes (last 30 years of the twenty-first century minus first 30 years of the observational period) for the ALL ensemble mean. Different columns of panels correspond to different seasons, as marked in the titles.

30 years of the observational period (1989–2018 minus 1901–30). The modeled patterns were computed for each of the 52 ALL simulations and the weighted mean of the resulting 52 patterns is what is shown in Fig. 7. For comparison, future changes are also shown (Figs. 7i–l), calculated using the last 30 years of the century (2071–2100 minus 1901–30). Although the observed patterns suggest an increase in variability when averaged over the entire area, they also appear to be largely influenced by noise. By contrast, the ensemble mean alleviates much of the noise effect, and reveals a more uniform increase of the variability in all seasons. The increase becomes more pronounced by the end of the century, is present in most parts of the continent, and is greater in winter than in summer.

Since the increase in variability according to the models is generally spatially uniform, we next examine how it varies with time for precipitation anomalies averaged over the whole European region. We construct the ensemble mean standard deviation time series for each experiment by computing the standard deviation of seasonal European mean precipitation in 30-yr rolling windows (Fig. 8). More specifically, for each 30-yr window we compute the standard deviation for each simulation of a given experiment and then use the resulting estimates to calculate the weighted mean. We also estimate the CTL standard deviation for the preindustrial climate in a similar way using equal time segments extracted from the CMIP6 models. While there is little change in the NAT climate, which is consistent with the CTL estimate, the greenhouse gas and aerosol forcings appear to drive variability in opposite directions, with the former leading to an increase and the latter to a decrease over time. The effect of individual forcings, however, is only indicative and is affected to some degree by natural fluctuations. With this limitation in mind, we find that as the GHG effect appears to dominate, the total response in the ALL experiment indicates an increase in variability that becomes evident after the 1950s in winter and spring, but only after the 2000s in the other seasons. The rate of change is also higher in the winter season. The summer time series suggest that summer variability may again decrease later in the century. However, this may be to some extent a manifestation of the effect of natural fluctuations. Indeed, we find that time series with three other SSPs do not indicate a definitive large future decrease in summer precipitation variability and, at least one scenario, points to a monotonic increase instead (Fig. S3 in the online supplemental material). We therefore conclude that according to the CMIP6 models

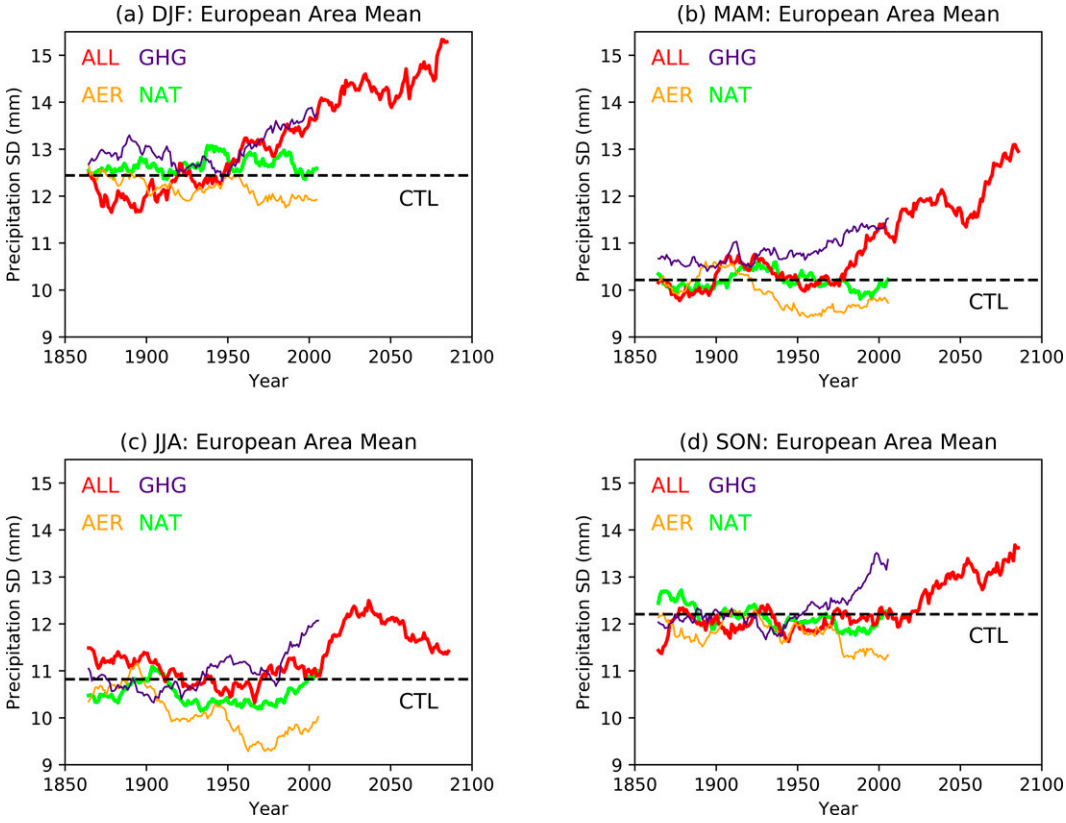

FIG. 8. Time series of the standard deviation of seasonal mean precipitation corresponding to the weighted ensemble mean of the ALL (red), GHG (purple), AER (orange), and NAT (green) experiments. The standard deviation values were calculated in 30-yr rolling windows from precipitation averaged over the European region. The standard deviation estimated from control simulations of the preindustrial climate is marked by the dashed black line. Different panels correspond to different seasons, as marked in the titles.

used here, seasonal variability is set to further increase over Europe, primarily due to the influence of greenhouse gas emissions.

Increases in precipitation variability have been identified before over a range spatial scales, for example, globally (Pendergrass et al. 2017) or in mid- and high latitudes, especially on seasonal time scales (Wood et al. 2021). However, the effect of small-scale processes in different regions and the interplay between dynamical and thermodynamical influences limit our understanding of the mechanisms that drive variability changes (van der Wiel and Bintanja 2021). In the northernmost parts of Europe, increased atmospheric moisture and its poleward transport have been suggested to lead to variability increases, while summer changes in the continent may also be sensitive to dynamical influences (O'Reilly et al. 2017). The important role of land–atmosphere interactions has also been identified as a contributor to variability increases, which manifests itself through a northward shift of climatic regimes in Europe (Seneviratne et al. 2006). Finally, oceanic warming in the North Atlantic may also exert significant influence on the winter variability in northwestern Europe (Årthun et al. 2017). Our findings provide further evidence of variability increases in all seasons under the effect of anthropogenic forcings, though the mechanisms through which the changes occur is subject to further research.

4. Optimal fingerprinting

Optimal fingerprinting (Allen and Stott 2003) is a well-established attribution methodology that underpins main attribution statements of the IPCC (Bindoff et al. 2013). Its application has also provided evidence of a detectable anthropogenic signal in precipitation changes on large spatial scales and changes in extremes (Wu et al. 2013; Zhang et al. 2007; Lambert et al. 2004; Min et al. 2011; Dong et al. 2021). The weaker anthropogenic effect on regional mean precipitation, however, makes its detection more challenging. Knutson and Zeng (2018) analyzed precipitation trend patterns in historical periods with a CMIP5 ensemble and identified significant changes in parts of Europe. Hoerling et al. (2012) also found a significant winter drying over the Mediterranean region relative to earlier years (pre-1970), when the anthropogenic influence was smaller. This study adds to the evidence of previous work by examining the detectability of the anthropogenic signal in seasonal European precipitation on the basis of a more rigorous fingerprinting analysis and its partitioning

between different forcings components. Fingerprinting can assess the detectability of the total climatic response to all external forcings, as well as the response to individual forcings, or forcing combinations. This partitioning of the response between its components is an advantage of the methodology, which has not yet been incorporated in newly developed techniques based on machine learning (Madakumbura et al. 2021).

Optimal fingerprinting is a generalized multivariate regression that expresses the observed change $\mathbf{y}$ as a linear combination of the responses to n external forcings (often referred to as fingerprints) $\mathbf{x}_i$, represented by the multimodel ensemble means of n different experiments:

$$\mathbf{y} = \sum_{i=1}^{n} (\mathbf{x}_i - \mathbf{u}_i)\beta_i + \mathbf{u}_0. \quad (1)$$

The noise terms $\mathbf{u}_i$ and $\mathbf{u}_0$ represent the effect of sampling noise (which becomes smaller as the ensemble size increases) and the effect of internal variability in the observations, respectively. One-way regression analyses with only a single fingerprint ($n = 1$) from the ALL experiment ($\mathbf{x}_{\mathrm{ALL}}$) assess the detectability of the climate's response to all external forcings in the observations. The total response may be decomposed further, and in this study we also carry out the following regressions:

1) We do a two-way regression analysis that separates the total anthropogenic (ANTHRO) and NAT responses. As common in fingerprinting analyses, responses to different forcings are assumed to combine linearly, hence the ANTHRO fingerprint, $\mathbf{x}_{\mathrm{ANTHRO}}$, is estimated as the difference between $\mathbf{x}_{\mathrm{ALL}}$ and $\mathbf{x}_{\mathrm{NAT}}$.
2) We do a two-way regression that separates the GHG fingerprint from the response to aerosols and all other anthropogenic and natural forcings (AER+OAN). The latter is estimated as the difference between $\mathbf{x}_{\mathrm{ALL}}$ and $\mathbf{x}_{\mathrm{GHG}}$.
3) We do a three-way regression that separates the GHG, AER, and OAN responses. The first two come from the corresponding GHG and AER experiments and the OAN from subtracting the GHG and AER fingerprints from the ALL.

The detectability of a fingerprint $\mathbf{x}_i$ in the observations is inferred by the corresponding scaling factor β_i. The scaling factors attempt to best match the fingerprints to the observed change and are reported as a best estimate and a 5%–95% uncertainty range. If the range does not include zero, the signal is deemed detectable, otherwise it is not distinguishable from internal variability. Moreover, scaling factors consistent with 1 indicate good consistency between the modeled response and the observed change, whereas scaling factors above or below 1 indicate that the modeled response is under- or overestimated.

The vectors representing the observed response ($\mathbf{y}$) and the fingerprints ($\mathbf{x}_i$) are constructed by concatenating the time series of decadal mean values of seasonal precipitation in the NEU and MED regions. Fingerprinting analyses employ this kind of spatial averaging to reduce dimensionality, as, for example, in the study of Wan et al. (2015), who split Northern Hemisphere's high latitudes into 1–6 regions. Here the two time series cover the observational period 1901–2018, which has 118 years in total. Therefore, when applying temporal averaging to compute decadal means, the last decade is incomplete and only includes 8 years, but this has no impact on the results as long as all data are processed the same way. The variance–covariance structure of the noise terms ($\mathbf{u}_i$, $\mathbf{u}_0$) is derived from 118-yr-long segments extracted from the CTL experiment, which are subsequently processed and organized into vectors, the same way as the observations and the model fingerprints. The regression is fitted using the total least squares method and the analysis is restricted to the subspace of the noise covariance defined by the 17 leading eigenvectors, which explain more than 75% of the observed variance. More details about the method can be found in Allen and Stott (2003).

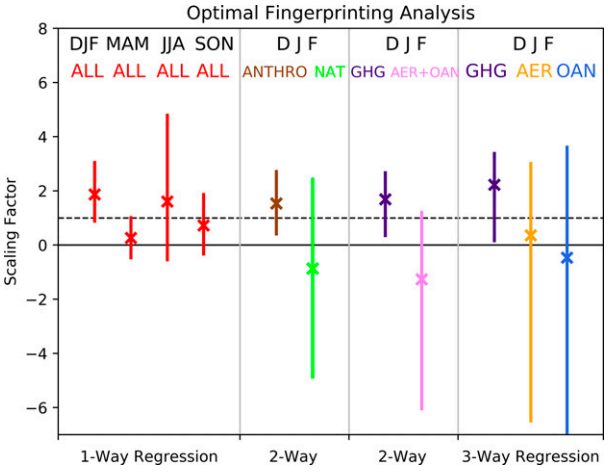

FIG. 9. Scaling factors and their 5%–95% uncertainty range from optimal fingerprinting analyses. Different segments of the figure present results from analyses that use fingerprints corresponding to different forcings or forcing combinations. Scaling factor values of zero (no detection) and unity are marked by the solid and dashed horizontal lines, respectively.

Results from the different optimal detection assessments carried out in this study are summarized in Fig. 9. We first examine whether the combined influence of anthropogenic and natural forcings is detectable and regress the ALL fingerprint against the observations. We conduct separate one-way regression analyses, one for each season. The resulting scaling factors are shown on the left part of Fig. 9. As noted above, winter changes in precipitation are more pronounced relative to other seasons, and consequently we find that the ALL fingerprint (dominated by the anthropogenic response) is only detected in winter. The winter scaling factor is consistent with 1, suggesting that the magnitude of the modeled forced response is consistent with the observations, although the uncertainty range of the scaling factor lies mostly above 1, which might indicate that the response is somewhat underestimated and needs to be scaled up to bring it in better agreement with the observations. As climate change escalates in coming years,

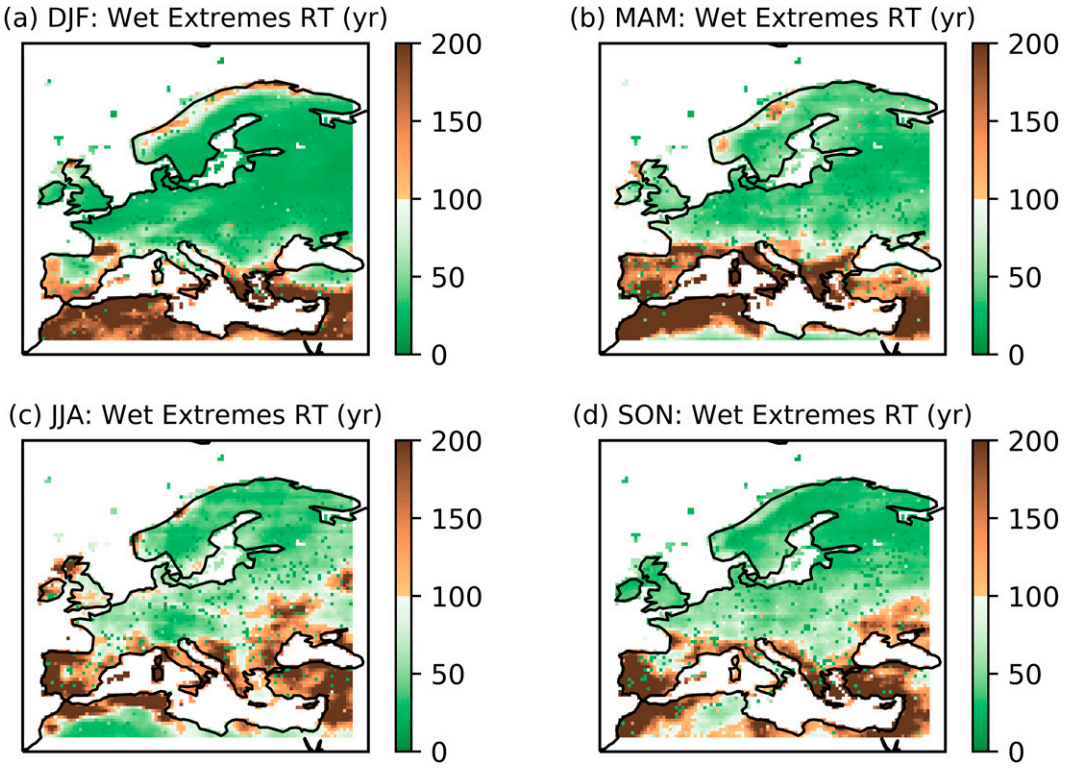

FIG. 10. Changes in the frequency of seasons with extremely high precipitation. The patterns show the present-day (years 2011–30) return time of extreme seasons that would occur once in a century without human influence on the climate. Green colors indicate an increase in the likelihood of such events, and brown colors indicate a decrease. Different panels correspond to different seasons, as marked in the titles.

its influence on precipitation could indeed become detectable in other seasons too, but for the rest of the detection analysis we only focus on winter, as we did not identify detectable signals in other seasons. Adverse socioeconomic impacts associated with changes in the winter climate of Europe (Schaller et al. 2016; Fuhrer et al. 2006) underline the need to understand better the role of human influence.

Winter precipitation changes seen in the ALL ensemble mean are mainly driven by anthropogenic forcings, as the effect of natural forcings is smaller and generally short-lived. It is therefore expected that the ANTHRO fingerprint is also likely to be detectable. This is confirmed with our two-way analysis (Fig. 9), which gives a scaling factor greater than zero and consistent with one for ANTHRO, but indicates no detection for NAT. The scaling factors of weak forcings (like NAT) have larger uncertainties, as it is harder to distinguish their effect from internal variability. The main contribution to the ANTHRO response, as seen in the previous Section, comes from greenhouse gas emissions and the second largest contribution from anthropogenic aerosols. Interestingly, the two forcings give rise to opposite changes, and previous work showed that the effect of both forcings on Northern Hemisphere's precipitation changes is detectable (Wu et al. 2013). A similar two-way detection analysis that attempts to distinguish between the GHG and AER+OAN responses shows that, in the case of winter precipitation changes in Europe, it is only the GHG fingerprint that can be clearly detected (Fig. 9). The availability of the AER experiment in CMIP6 also allows us to carry out a three-way regression and examine the effects of GHG, AER, and OAN separately. As before, the GHG effect can still be detected, but this is not the case for AER, or for other weaker forcings (Fig. 9). On the basis of our fingerprinting analysis, we conclude that greenhouse gas emissions have led to precipitation changes since the beginning of the twentieth century that have risen significantly above internal variability and can be detected in the observations.

5. Changes in extremes

a. *Patterns of changes in extremes*

So far, we examined changes in the seasonal mean precipitation driven by external forcings. In the last part of the study, we shift the focus on changes in extremely wet and dry seasons, more likely to be associated with high-impact floods and droughts. We stress that wet and dry seasons are only described here in terms of rainfall, which offers a limited perspective on complex events like droughts. We employ a risk-based framework, common in event attribution studies (Herring et al. 2021), that determines the anthropogenic influence on the likelihood of extreme events from ensembles of simulations with and without human influence (Stott et al. 2016). We first consider extremely wet and dry seasons that

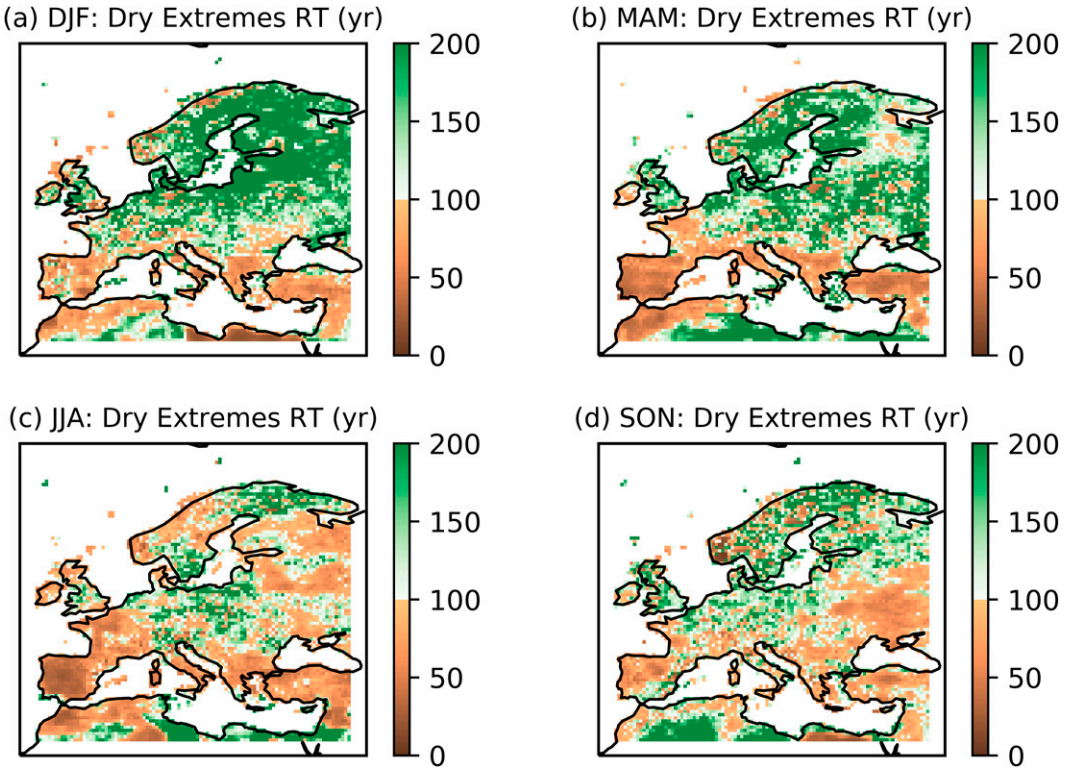

FIG. 11. Changes in the frequency of seasons with extremely low precipitation. The patterns show the present-day (years 2011–30) return time of extreme seasons that would occur once in a century without human influence on the climate. Green colors indicate a decrease in the likelihood of such events, and brown colors indicate an increase. Different panels correspond to different seasons, as marked in the titles.

are rare in the natural climate, occurring on average 1 every 100 years, and then estimate how their likelihood has changed in the present climate, represented by the period 2011–30.

Maps showing the return time patterns of seasons with low and high precipitation anomalies are constructed as follows. First, we estimate the 1st (dry events) and 99th (wet events) percentiles of the precipitation anomaly (i.e., seasons with 100 ears return time) in the NAT climate. At each grid box we have data from 56 NAT simulations that cover a period of 171 years, so in total we have samples of 9576 anomalies for the computation of the percentiles. These are used to define extreme events and we next estimate the probability of seasons with precipitation below the 1st percentile and above the 99th percentile in the present climate. Extreme probabilities are calculated with the generalized Pareto distribution, applied to anomaly samples extracted from the 52 ALL simulations over the period 2011–30. The calculations are carried out on every grid box, and the resulting patterns of the present-day return time are illustrated in Figs. 10 (wet events) and 11 (dry events).

We note again a contrast in the changing likelihood of extreme seasons between the Mediterranean basin and the rest of the continent. Seasons with extremely high precipitation anomalies (Fig. 10) become much rarer in the MED where their return time has more than doubled relative to the natural world in many parts of the region. Such wet seasons, however, are now estimated to occur more frequently over the rest of Europe, especially in winter, when their return time reduces to a few decades in most areas. On the other hand, seasons with extremely low precipitation anomalies (Fig. 11) become more common in the south and less common in the north of the European regions. The increase in the likelihood of dry events is more widespread in autumn, and especially summer, when it appears to affect most European areas. The changes in extremes are consistent with the trends in precipitation discussed in section 3, but are also influenced by changes in variability, as, for example, increases in the spread of the distributions could increase the likelihood of extremes.

b. Past, present, and future extremes in NEU and MED

We also estimate the return time of seasons with very high or low precipitation averaged over the NEU and MED regions. Using again data from the ALL and NAT experiments, we estimate the probabilities of events with regional mean precipitation anomalies above (wet) or below (dry) prespecified return levels. We carry out the computations over a range of return levels and present the resulting return level minus return time plots in Figs. 12 and 13. Probabilities are estimated for the NAT climate (using all simulated years of the NAT experiment), the present climate (ALL years 2011–30) and the climate of the end of the century (years 2081–2100). Uncertainties in the return times are estimated with a

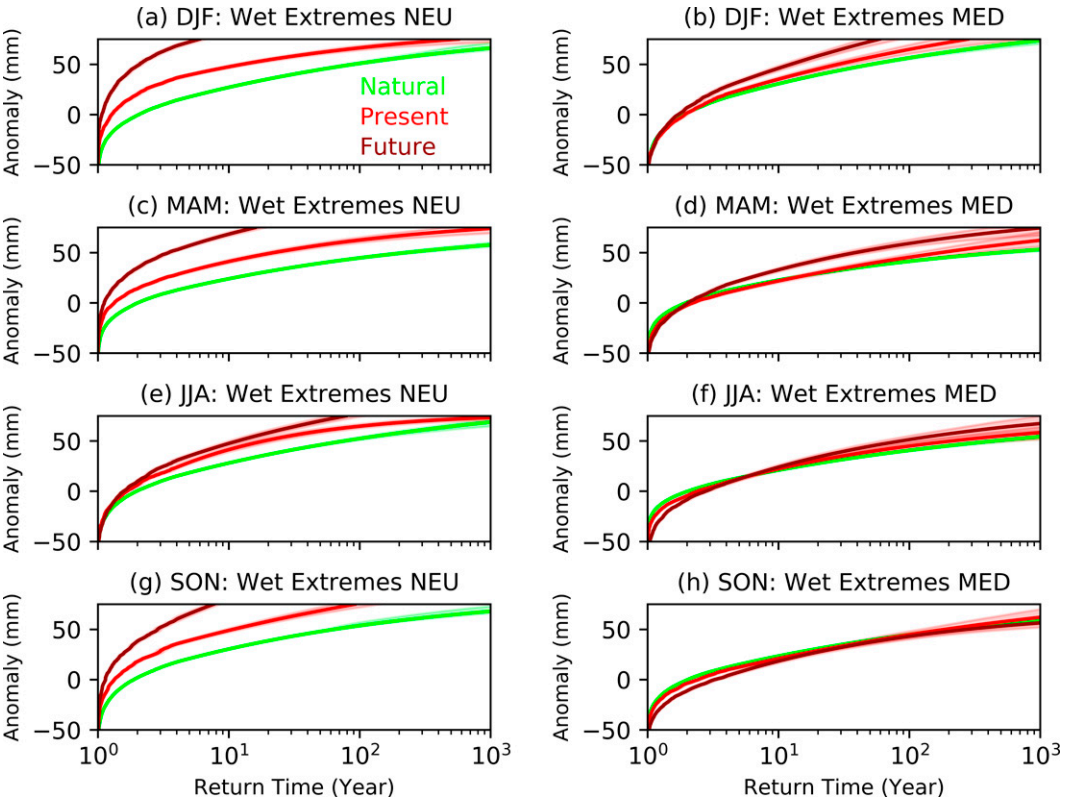

FIG. 12. Return time (inverse probability) of wet seasons corresponding to different levels of seasonal precipitation anomalies in (a),(c),(e),(g) NEU and (b),(d),(f),(g) MED estimated for the NAT climate without the effect of human influence (green), the present climate (red), and the climate of the late twenty-first century (dark red). Different rows of panels correspond to different seasons, as marked in the titles.

bootstrapping procedure and represented by the colored areas in Figs. 12 and 13, but as the samples used for the probability estimation are large, the uncertainties are generally small and not easy to distinguish from the best estimate. We find a marked decrease in the return time of extremely wet seasons in NEU in all seasons under the influence of anthropogenic forcings and a more moderate decrease in the MED in winter and spring (Fig. 12). Conversely, human influence is shown to decrease the frequency of extremely dry seasons in NEU (return time increases) and, apart from winter, increase the frequency in the MED (Fig. 13). In conclusion, we find that wet extremes become more frequent in NEU and dry extremes become less frequent in NEU and more frequent in MED due to human influence on the climate. Similar to changes in the mean precipitation, changes in extremes may be more of thermodynamical origin in the south (where convection processes are stronger) and dynamical in the north, but, again, further research is needed to elucidate the mechanisms behind the difference in the response across the Europe.

6. Discussion

Results from our attribution study with an ensemble of the latest CMIP6 models offer valuable insights on the contribution of anthropogenic forcings to changes in European precipitation since the 1850s and into coming decades. A characteristic pattern of emerging trends is evident in all seasons, comprising increases in precipitation north of the Mediterranean basin and decreases in the southernmost parts of the continent. The pattern is stronger and more widespread in winter, but weaker in summer when, apart from the MED, large areas in eastern and western Europe also experience drier conditions. Models suggest that much of the change is driven by greenhouse gas emissions, while anthropogenic aerosols favor an opposite response. It may thus be expected that as European aerosol emissions continue to decrease, the greenhouse gas influence will strengthen in coming years (Folini and Wild 2011; Samset et al. 2018).

Because the influence of anthropogenic forcings is stronger in winter, it is more likely to be detectable than in other seasons. Indeed, we demonstrate that on the basis of an optimal fingerprinting analysis, both the anthropogenic signal in winter, but also its greenhouse gas component, is detected in the observations. This is the first demonstration of a detectable greenhouse gas signal for mean rainfall changes on continental scales. Despite the weakening of the greenhouse gas signal by the effect of aerosols, its detection is still feasible, and an interesting future research question to consider is whether, going forward, detection becomes possible in other seasons too.

Greenhouse gas emissions are also found to increase the variability of seasonal rainfall over most of Europe. It should be

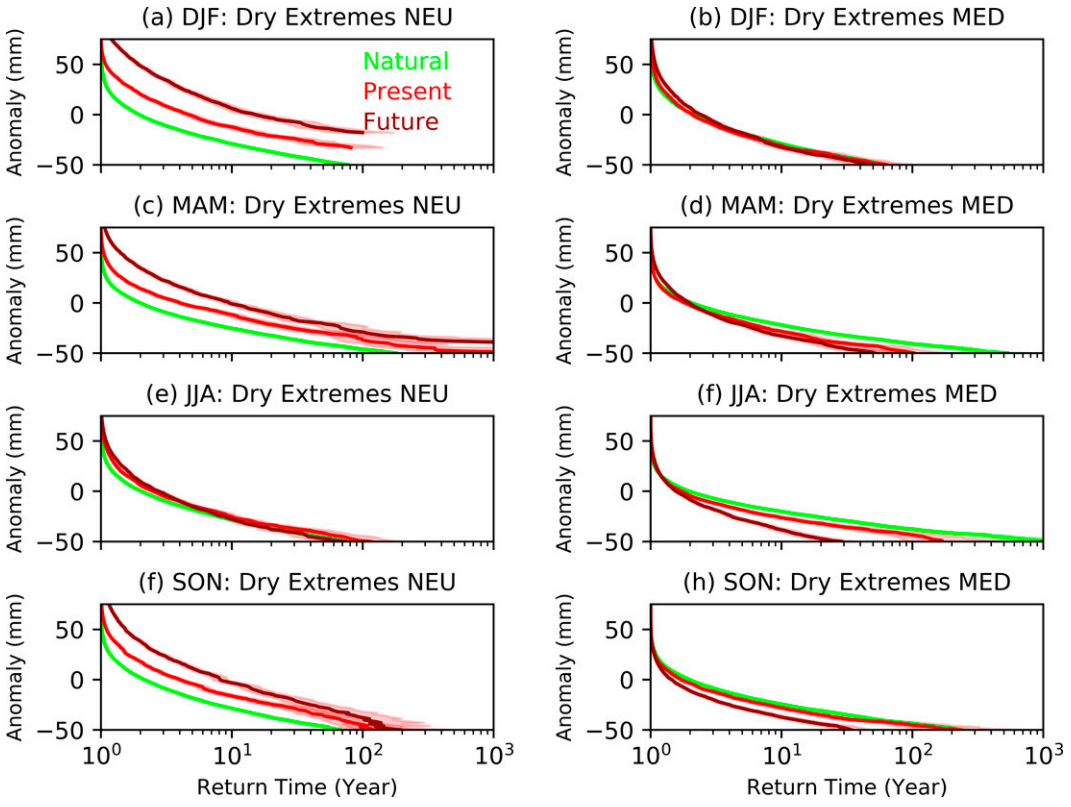

FIG. 13. As in Fig. 12, but for dry seasons.

stressed that our analysis only provides a first indication of this change and although the strong effect of natural fluctuations precludes a precise quantification of its magnitude, we can still see an emerging signal in the CMIP6 simulations. Increasing variability would have possible repercussions for extremes. For example, while summer precipitation is found to decrease over France, wet extremes are suggested to have become more frequent, which could manifest the effect of an increase in variability. Here we only examine seasonal precipitation extremes and find an increasing risk of extremely dry seasons in the Mediterranean basin and extremely wet seasons elsewhere in the European region. More detailed research into of the risk of floods would require streamflow information, for example, from hydrological models. Similarly, drought studies should also account for a range of other relevant variables like temperature, wind, humidity, and radiation. Precipitation, however, still remains an underlying main driver and it is vital to understand how it changes in a warming world. Therefore, our analysis offers a useful broader perspective of large-scale seasonal precipitation changes, elucidating the context in which high-impact events develop. Such attribution information contributes to the scientific basis that decision-makers can use to frame effective mitigation policies and adaptation planning.

Acknowledgments. This work was supported by the Met Office Hadley Centre Climate Programme funded by BEIS and Defra.

Data availability statement. CRU TS4.03 gridded precipitation data are available from the CEDA archive (https://archive.ceda.ac.uk/). Data from different experiments with the CMIP6 models used in the study can be downloaded from nodes of the ESGF (https://esgf.llnl.gov/).

REFERENCES

Alexander, L. V., 2016: Global observed long-term changes in temperature and precipitation extremes: A review of progress and limitations in IPCC assessments and beyond. *Wea. Climate Extremes*, **11**, 4–16, https://doi.org/10.1016/j.wace.2015.10.007.

Allan, R. P., 2014: Dichotomy of drought and deluge. *Nat. Geosci.*, **7**, 700–701, https://doi.org/10.1038/ngeo2243.

Allen, M. R., and W. J. Ingram, 2002: Constraints on future changes in climate and the hydrologic cycle. *Nature*, **419**, 228–232, https://doi.org/10.1038/nature01092.

——, and P. A. Stott, 2003: Estimating signal amplitudes in optimal fingerprinting, part I: Theory. *Climate Dyn.*, **21**, 477–491, https://doi.org/10.1007/s00382-003-0313-9.

Årthun, M., T. Eldevik, E. Viste, H. Drange, T. Furevik, H. L. Johnson, and N. S. Keenlyside, 2017: Skillful prediction of northern climate provided by the ocean. *Nat. Commun.*, **8**, 15875, https://doi.org/10.1038/ncomms15875.

Barcikowska, M. J., S. B. Kapnick, L. Krishnamurty, S. Russo, A. Cherchi, and C. K. Folland, 2020: Changes in the future summer Mediterranean climate: Contribution of teleconnections

and local factors. *Earth Syst. Dyn.*, **11**, 161–181, https://doi.org/10.5194/esd-11-161-2020.

Bhend, J., and P. Whetton, 2013: Consistency of simulated and observed regional changes in temperature, sea level pressure and precipitation. *Climatic Change*, **118**, 799–810, https://doi.org/10.1007/s10584-012-0691-2.

Bindoff, N. L., and Coauthors, 2013: Detection and attribution of climate change: From global to regional. *Climate Change 2013: The Physical Science Basis*, T. F. Stocker et al., Eds., Cambridge University Press, 867–952.

Bock, L., and Coauthors, 2020: Quantifying progress across different CMIP phases with the ESMValTool. *J. Geophys. Res. Atmos.*, **125**, e2019JD032321, https://doi.org/10.1029/2019JD032321.

Brogli, R., S. Lund Sørland, N. Kröner, and C. Schär, 2019: Causes of future Mediterranean precipitation decline depend on the season. *Environ. Res. Lett.*, **14**, 114017, https://doi.org/10.1088/1748-9326/ab4438.

Chen, H., and J. Sun, 2017: Contribution of human influence to increased daily precipitation extremes over China. *Geophys. Res. Lett.*, **44**, 2436–2444, https://doi.org/10.1002/2016GL072439.

Christidis, N., and P. A. Stott, 2021: The influence of anthropogenic climate change on wet and dry summers in Europe. *Sci. Bull.*, **66**, 813–823, https://doi.org/10.1016/j.scib.2021.01.020.

——, ——, A. Scaife, A. Arribas, G. S. Jones, D. Copsey, J. R. Knight, and W. J. Tennant, 2013: A new HadGEM3-A based system for attribution of weather and climate-related extreme events. *J. Climate*, **26**, 2756–2783, https://doi.org/10.1175/JCLI-D-12-00169.1.

Dong, S., Y. Sun, C. Li, X. Zhang, S.-K. Min, and Y.-H. Kim, 2021: Attribution of extreme precipitation with updated observations and CMIP6 simulations. *J. Climate*, **34**, 871–881, https://doi.org/10.1175/JCLI-D-19-1017.1.

Dottori, F., and Coauthors, 2018: Increased human and economic losses from river flooding with anthropogenic warming. *Nat. Climate Change*, **8**, 781–786, https://doi.org/10.1038/s41558-018-0257-z.

Eyring, V., S. Bony, G. A. Meehl, C. A. Senior, B. Stevens, R. J. Stouffer, and K. E. Taylor, 2016: Overview of the Coupled Model Intercomparison Project Phase 6 (CMIP6) experimental design and organization. *Geosci. Model Dev.*, **9**, 1937–1958, https://doi.org/10.5194/gmd-9-1937-2016.

——, and Coauthors, 2021: Human influence on the climate system. *Climate Change 2021: The Physical Science Basis*, V. Masson-Delmotte et al., Eds., Cambridge University Press, 423–552, https://www.ipcc.ch/report/ar6/wg1/downloads/report/IPCC_AR6_WGI_Chapter03.pdf.

Folini, D., and M. Wild, 2011: Aerosol emissions and dimming/brightening in Europe: Sensitivity studies with ECHAM5-HAM. *J. Geophys. Res.*, **116**, D21104, https://doi.org/10.1029/2011JD016227.

Folland, C. K., J. Knight, H. W. Linderholm, D. Fereday, S. Ineson, and J. W. Hurrell, 2009: The summer North Atlantic Oscillation: Past, present, and future. *J. Climate*, **22**, 1082–1103, https://doi.org/10.1175/2008JCLI2459.1.

Fuhrer, J., M. Beniston, A. Fischlin, C. Frei, S. Goyette, K. Jasper, and C. Pfister, 2006: Climate risks and their impact on agriculture and forests in Switzerland. *Climate Variability, Predictability and Climate Risks*, H. Wanner et al., Eds., Springer, 79–102, https://doi.org/10.1007/978-1-4020-5714-4_5.

Gillett, N., M. R. Allen, and S. F. B. Tett, 2000: Modelled and observed variability in atmospheric vertical temperature structure. *Climate Dyn.*, **16**, 49–61, https://doi.org/10.1007/PL00007921.

Giorgi, F., and R. Francisco, 2000: Uncertainties in regional climate change prediction: A regional analysis of ensemble simulations with the HADCM2 coupled AOGCM. *Climate Dyn.*, **16**, 169–182, https://doi.org/10.1007/PL00013733.

Harris, I., T. J. Osborn, P. Jones, and D. Lister, 2020: Version 4 of the CRU TS monthly high-resolution gridded multivariate climate dataset. *Sci. Data*, **7**, 109, https://doi.org/10.1038/s41597-020-0453-3.

Held, I. M., and B. J. Soden, 2006: Robust responses of the hydrological cycle to global warming. *J. Climate*, **19**, 5686–5699, https://doi.org/10.1175/JCLI3990.1.

Herring, S. C., N. Christidis, A. Hoell, M. P. Hoerling, and P. A. Stott, Eds., 2021: Explaining Extreme Events of 2019 from a Climate Perspective. *Bull. Amer. Meteor. Soc.*, 102 (1), S1–S112, https://doi.org/10.1175/BAMS-ExplainingExtremeEvents2019.1.

Hoerling, M., J. Eischeid, J. Perlwitz, X. Quan, T. Zhang, and P. Pegion, 2012: On the increased frequency of Mediterranean drought. *J. Climate*, **25**, 2146–2161, https://doi.org/10.1175/JCLI-D-11-00296.1.

Hurrell, J. W., Y. Kushnir, G. Ottersen, and M. Visbeck, 2003: *The North Atlantic Oscillation: Climatic Significance and Environmental Impact. Geophys. Monogr.*, Vol. 134, Amer. Geophys. Union, 279 pp., https://doi.org/10.1029/GM134.

Iturbide, M., and Coauthors, 2020: An update of IPCC climate reference regions for subcontinental analysis of climate model data: Definition and aggregated datasets. *Earth Syst. Sci. Data*, **12**, 2959–2970, https://doi.org/10.5194/essd-12-2959-2020.

Jakob, C., 2014: Going back to basics. *Nat. Climate Change*, **4**, 1042–1045, https://doi.org/10.1038/nclimate2445.

Jones, G. S., P. A. Stott, and N. Christidis, 2013: Attribution of observed historical near–surface temperature variations to anthropogenic and natural causes using CMIP5 simulations. *J. Geophys. Res. Atmos.*, **118**, 4001–4024, https://doi.org/10.1002/jgrd.50239.

Kirchmeier-Young, M. C., and X. Zhang, 2020: Human influence has intensified extreme precipitation in North America. *Proc. Natl. Acad. Sci. USA*, **117**, 13 308–13 313, https://doi.org/10.1073/pnas.1921628117.

Knutson, T. R., and F. Zeng, 2018: Model assessment of observed precipitation trends over land regions: Detectable human influences and possible low bias in model trends. *J. Climate*, **31**, 4617–4637, https://doi.org/10.1175/JCLI-D-17-0672.1.

Kumar, S., R. P. Allan, F. Zwiers, D. M. Lawrence, and P. A. Dirmeyer, 2015: Revisiting trends in wetness and dryness in the presence of internal climate variability and water limitations over land. *Geophys. Res. Lett.*, **42**, 10 867–10 875, https://doi.org/10.1002/2015GL066858.

Lambert, F. H., P. A. Stott, M. R. Allen, and M. A. Palmer, 2004: Detection and attribution of changes in 20th century land precipitation. *Geophys. Res. Lett.*, **31**, L10203, https://doi.org/10.1029/2004GL019545.

Li, X., Z.-Z. Hu, X. Jiang, Y. Li, Z. Gao, S. Yang, J. Zhu, and B. Jha, 2016: Trend and seasonality of land precipitation in observations and CMIP5 model simulations. *Int. J. Climatol.*, **36**, 3781–3793, https://doi.org/10.1002/joc.4592.

Madakumbura, G. D., C. W. Thackeray, J. Norris, N. Goldenson, and A. Hall, 2021: Anthropogenic influence on extreme precipitation over global land areas seen in multiple observational datasets. *Nat. Commun.*, **12**, 3944, https://doi.org/10.1038/s41467-021-24262-x.

Min, S.-K., X. Zhang, F. W. Zwiers, and G. C. Hegerl, 2011: Human contribution to more-intense precipitation extremes. *Nature*, **470**, 378–381, https://doi.org/10.1038/nature09763.

O'Reilly, C. H., T. Woollings, and L. Zanna, 2017: The dynamical influence of the Atlantic multidecadal oscillation on continental climate. *J. Climate*, **30**, 7213–7230, https://doi.org/10.1175/JCLI-D-16-0345.1.

Padrón, R. S., and Coauthors, 2020: Observed changes in dry-season water availability attributed to human-induced climate change. *Nat. Geosci.*, **13**, 477–481, https://doi.org/10.1038/s41561-020-0594-1.

Pendergrass, A. G., F. Lehner, B. M. Sanderson, and Y. Xu, 2015: Does extreme precipitation intensity depend on the emissions scenario? *Geophys. Res. Lett.*, **42**, 8767–8774, https://doi.org/10.1002/2015GL065854.

——, R. Knutti, F. Lehner, C. Deser, and B. M. Sanderson, 2017: Precipitation variability increases in a warmer climate. *Sci. Rep.*, **7**, 17966, https://doi.org/10.1038/s41598-017-17966-y.

Polson, D., and G. C. Hegerl, 2017: Strengthening contrast between precipitation in tropical wet and dry regions. *Geophys. Res. Lett.*, **44**, 365–373, https://doi.org/10.1002/2016GL071194.

Priestley, M. D. K., D. Ackerley, J. L. Catto, K. I. Hodges, R. E. McDonald, and R. W. Lee, 2020: An overview of the extratropical storm tracks in CMIP6 historical simulations. *J. Climate*, **33**, 6315–6343, https://doi.org/10.1175/JCLI-D-19-0928.1.

Riahi, K., and Coauthors, 2017: The shared socioeconomic pathways and their energy, land use, and greenhouse gas emissions implications: An overview. *Global Environ. Change*, **42**, 153–168, https://doi.org/10.1016/j.gloenvcha.2016.05.009.

Samset, B. H., M. Sand, C. J. Smith, S. E. Bauer, P. M. Forster, J. S. Fuglestvedt, S. Osprey, and C.-F. Schleussner, 2018: Climate impacts from a removal of anthropogenic aerosol emissions. *Geophys. Res. Lett.*, **45**, 1020–1029, https://doi.org/10.1002/2017GL076079.

Sarojini, B., P. A. Stott, and E. Black, 2016: Detection and attribution of human influence on regional precipitation. *Nat. Climate Change*, **6**, 669–675, https://doi.org/10.1038/nclimate2976.

Scaife, A. A., and Coauthors, 2012: Climate change projections and stratosphere–troposphere interaction. *Climate Dyn.*, **38**, 2089–2097, https://doi.org/10.1007/s00382-011-1080-7.

Schaller, N., and Coauthors, 2016: Human influence on climate in the 2014 southern England winter floods and their impacts. *Nat. Climate Change*, **6**, 627–634, https://doi.org/10.1038/nclimate2927.

Screen, J. A., 2013: Influence of Arctic sea ice on European summer precipitation. *Environ. Res. Lett.*, **8**, 044015, https://doi.org/10.1088/1748-9326/8/4/044015.

Seager, R. J., N. Naik, and G. C. Hegerl, 2010: Thermodynamic and dynamic mechanisms for large-scale changes in the hydrological cycle in response to global warming. *J. Climate*, **23**, 4651–4668, https://doi.org/10.1175/2010JCLI3655.1.

Seneviratne, S. I., D. Lüthi, M. Litschi, and C. Schär, 2006: Land-atmosphere coupling and climate change in Europe. *Nature*, **443**, 205–209, https://doi.org/10.1038/nature05095.

Slivinski, L. C., and Coauthors, 2019: Towards a more reliable historical reanalysis: Improvements for version 3 of the Twentieth Century Reanalysis system. *Quart. J. Roy. Meteor. Soc.*, **145**, 2876–2908, https://doi.org/10.1002/qj.3598.

Stott, P. A., and Coauthors, 2016: Attribution of extreme weather and climate-related events. *Wiley Interdiscip. Rev. Climate Change*, **7**, 23–41, https://doi.org/10.1002/wcc.380.

Taylor, K. E., R. J. Stouffer, and G. A. Meehl, 2012: An overview of CMIP5 and the experiment design. *Bull. Amer. Meteor. Soc.*, **93**, 485–498, https://doi.org/10.1175/BAMS-D-11-00094.1.

Trenberth, K. E., 2011: Changes in precipitation with climate change. *Climate Res.*, **47**, 123–138, https://doi.org/10.3354/cr00953.

van der Wiel, K., and R. Bintanja, 2021: Contribution of climatic changes in mean and variability to monthly temperature and precipitation extremes. *Commun. Earth Environ.*, **2**, 1, https://doi.org/10.1038/s43247-020-00077-4.

Vannière, B., and Coauthors, 2019: Multi-model evaluation of the sensitivity of the global energy budget and hydrological cycle to resolution. *Climate Dyn.*, **52**, 6817–6846, https://doi.org/10.1007/s00382-018-4547-y.

Wan, H., X. Zhang, F. Zwiers, and S.-K. Min, 2015: Attributing northern high-latitude precipitation change over the period 1966–2005 to human influence. *Climate Dyn.*, **45**, 1713–1726, https://doi.org/10.1007/s00382-014-2423-y.

Westervelt, D. M., and Coauthors, 2018: Connecting regional aerosol emissions reductions to local and remote precipitation responses. *Atmos. Chem. Phys.*, **18**, 12 461–12 475, https://doi.org/10.5194/acp-18-12461-2018.

Wilhite, D. A., M. D. Svoboda, and M. J. Hayes, 2007: Understanding the complex impacts of drought: A key to enhancing drought mitigation and preparedness. *Water Resour. Manage.*, **21**, 763–774, https://doi.org/10.1007/s11269-006-9076-5.

Wood, R. R., F. Lehner, A. G. Pendergrass, and S. Schlunegger, 2021: Changes in precipitation variability across time scales in multiple global climate model large ensembles. *Environ. Res. Lett.*, **16**, 084022, https://doi.org/10.1088/1748-9326/ac10dd.

Wu, P., N. Christidis, and P. A. Stott, 2013: Anthropogenic impact on the Earth's hydrological cycle. *Nat. Climate Change*, **3**, 807–810, https://doi.org/10.1038/nclimate1932.

Zhang, X., F. W. Zwiers, G. C. Hegerl, F. H. Lambert, N. P. Gillett, S. Solomon, P. A. Stott, and T. Nozawa, 2007: Detection of human influence on twentieth-century precipitation trends. *Nature*, **448**, 461–465, https://doi.org/10.1038/nature06025.